P3.1 CONTRIBUTIONS FROM CALIFORNIA COASTAL- ZONE SURFACE FLUXES TO HEAVY COASTAL PRECIPITATION: A CASE STUDY FROM AN EL NIÑO YEAR

P. Ola G. Persson[1], P. J. Neiman[2], B. Walter[3], and F. M. Ralph[2]
[1]Cooperative Institute for Research in Environmental Sciences/NOAA/ETL, Boulder, CO
[2]NOAA/Environmental Technology Laboratory, Boulder, CO
[3]NorthWest Research Associates, Bellevue, WA

1. OBJECTIVES

Assess contribution from California coastal surface fluxes to heavy coastal precipitation for a storm during an El Niño year

Extend the results to assess the contribution during non-El Niño years

2. DATA SET AND SYNOPTIC/ MESOSCALE DESCRIPTION

Data set

California Landfalling Jets Experiment (CALJET; Nov. 1997- March 1998)

Large integrated CALJET observational network (Fig. 1) included
- NOAA P-3 aircraft (in-situ, LF radar, Doppler tail radar, dropsondes)
- coastal array of 915 MHz wind profilers

Case of Feb. 2-3, 1998; landfall occurred on Feb. 3 09 - 20 UTC
- coastal sea-surface temperature (SST) anomalies of +1.5-2.5°C (Fig.2)

Feb. 3 P-3 flight: 1140-1930 UTC (Fig.2)
- in the Santa Barbara Channel at 1230-1300 UTC: low-level
- 140 km further south at 1330-1605 UTC: dropsonde cross-section followed by low-level flux stack
- in the Santa Barbara Channel at 1630-1800 UTC: low-level

Synoptic description

Cyclogenesis occurred 1000 km offshore on Feb. 2
- -complex mesoscale structure and a 40 m/s low-level jet (LLJ) at 1 km
- -low deepened as it approached the California coastline
- -system consisted of a prefrontal squall line, a primary front and a secondary front (Fig. 1)

Upon landfall on Feb. 3, complex interactions occurred between the coastal orography in the California Bight region and the storm (Neiman *et al.*, 2003)
- primary cold front retarded below 850 mb by coastal blocking effects near 0830-1100 UTC, splitting primary front
- in the Santa Barbara Channel, secondary cold front merged with remnant low-level cold front near 1600 UTC

Precipitation in excess of 300 mm (12 inches) fell in 24 h in some areas of the Southern California coastal mountains, resulting in flooding and mudslides. The storm also forced the closure of Los Angeles International Airport.
- the prefrontal squall line and the primary cold front brought the initial heavy precipitation
- the secondary cold front produced brief but very intense precipitation in the coastal mountains along the northern shore of the California Bight (Fig.1) – **THE PRECIPITATION OF CONCERN FOR THIS STUDY**

Sampling of pre-secondary cold frontal air

Detailed in-situ thermodynamic and flux measurements were obtained in the 15-20 m/s LLJ ahead of the secondary front about 140 km offshore between 1430-1605 UTC and later near the shore between 1730-1830 UTC.

Offshore measurements (1430-1605 UTC):
- -bubble of warm, moist air ahead of the secondary cold front (Fig. 3a), with a weak warm-frontal feature to the east

Shoreward advection: In the 2.5 hours between the offshore and nearshore measurements, this bubble of warm, moist air advected towards the coast to the NNE, keeping just to the east of the secondary cold front. This is illustrated schematically in Fig. 4. Hence, the nearshore sampling by the P-3 occurred in approximately the same air that was sampled offshore.

Nearshore measurements along the line S-S' in Fig. 4: Analysis (Fig. 3b) represents the nearshore environment after the merger of the secondary cold front with the low-level remnant of the primary cold-front. This analysis shows the warm, moist bubble of air still ahead of the secondary cold front.

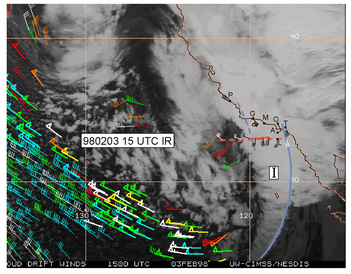

Fig. 1: IR image and mid-level cloud-track winds at 1500 UTC Feb. 3, 1998. The primary (solid) and secondary (dashed) cold fronts are shown in blue. The dashed red line shows the approximate track of the P-3 aircraft between 1300-1605 UTC, while the wind flags on this track show low-level winds measured in-situ or by dropsondes. The coastal wind profiler sites of Pt. Piedras Blancas (P), Goleta (G), Santa Catalina (A), Oxnard (O), and Tustin (T) are shown, with low-level winds shown at four of these sites. The Pt. Mugu (M) rawinsonde site is also shown.

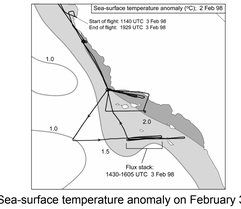

Fig. 2: Sea-surface temperature anomaly on February 3, 1998 along the southern California coastline. Also shown is the P-3 flight track (heavy line with arrows) from 1140-1930 UTC on Feb. 3.

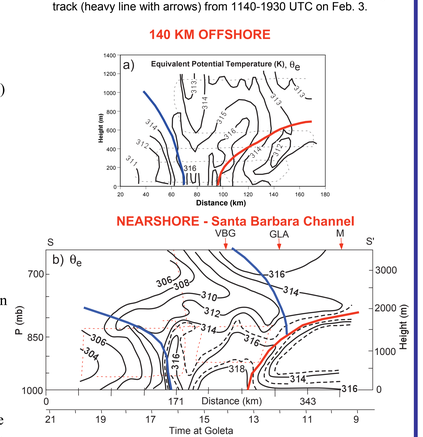

Fig. 3: a) Offshore and b) nearshore θ_e cross-sections. In a), a velocity of 16.8 ms^{-1} from 200° was used in the time-to-space conversion of the aircraft data. In b), the analysis was done using the aircraft data collected near 1230 UTC and near 1730 UTC, data from buoys in the Santa Barbara Channel and 3 rawinsondes from Goleta and Pt. Mugu (arrows). A velocity of 9.2 m/s from 270° was used in the time-to-space conversion. The location of b) is marked by S-S' in Fig. 4. The aircraft tracks are shown as faint dashed lines.

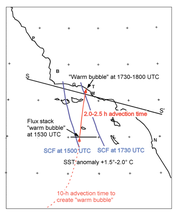

Fig 4: Schematic of the parcel trajectory from the offshore cross-section to the north coast of the California Bight. The heavy blue lines represent the secondary cold front at the two times indicated. The line S-S' shows the location of the nearshore cross section in Fig. 3b.

3. FLUXES AND FLUX IMPACT

Flux calculations

Flux stack: 1430-1605 UTC, ahead of the secondary cold front,140 km south of the coastline near Goleta (Figs. 2, 4)
- 5 level aircraft passes (or legs) approximately perpendicular to the frontal orientation and the low-level winds
- legs done in descending order between 1154 m and 66 m (Fig. 3a)
- standard 1-s flight level measurements
- 40 Hz data to observe turbulent structures down to a scale of about 5 m

Fluxes of sensible (H_s) and latent (H_l) heat and stress (τ) calculated from covariance technique along each leg. Only H_s and H_l discussed here. Because of the presence of the two frontal features, length of homogeneous sampling legs only half of 60 km length for ideal statistical sampling

Results of offshore warm-sector flux stack (Table 1):
a) boundary layer (BL) depth is approximately 600 m, as seen by the profiles of virtual potential temperature (θ_v) and the specific humidity (q), and by location of wind speed maximum near this height.
b) surface layer (SL), where the fluxes should be approximately constant with height, about 60 m deep (10% of BL)
- hence, lowest flux leg near top of SL

Table 1: *Flux measurements in the offshore warm sector. The values are means for the 26-34 km long legs, where the length is given by "xs-xe". The surface temperature is given by an airborne expendable bathythermograph(AXBT) and the downward-looking radiometer, while the surface mixing ratio is computed assuming saturated conditions.*

Time	Height	xs-xe	<p>	<T>	<q>	<θ_v>	<θ_e>s	<ws>	<wd>	H_l	H_s	τ
UTC	m	km	mb	C	g/kg	K	K	m/s	deg	W/m^2	W/m^2	N/m^2
152016 AXBT	0	96		15.73				0	-	-	-	-
155250-155700	0	69-98	993.6	15.8	11.44	291.5	321.7	0	-	-	-	-
155250-155700	66	69-98	985.7	14.9	9.47	290.9	316	13.4	198	32.1	12.1	0.09
153100-153518	285	75-102	960.5	13.15	9.09	291.2	315.4	14.8	197	42	-6	0.05
151900-152400	427	70-104	944.3	12.29	8.89	291.7	315.4	15.6	195	113.6	-47	0.19
145300-145700	590	76-102	926.5	11.22	8.38	292.1	314.6	16.6	198	2.5	-12.1	0.06
144600-145000	1154	73-102	866.6	8.1	6.95	294.2	313.2	13.9	194	32	6	-0.03

Effects of surface fluxes on BL

METHOD 1: Assume that fluxes below 66 m are the same as at 66 m, and that the fluxes at the different heights remain constant in time as the air parcel translates towards the coast. The flux divergence for each layer then gives the change for that layer, and the average change of a parameter for the entire boundary layer is the layer-weighted mean of the changes over the depth of the boundary layer. The changes for each layer and for the entire boundary layer using this method are seen as (WM) in Table 2.

METHOD 2: Assume that the surface fluxes are given by those measured at 66 m, and that the fluxes are approximately zero at the top of the boundary layer. Hence, the flux divergence and the mean change in the boundary layer can be calculated. These results are given as (L1) in Table 2.

RESULTS (Table 2): Both methods give nearly identical results for the specific humidity; that is, that the BL specific humidity increases by only about 0.15-0.2 g kg^{-1}. The temperature is expected to increase by either 0.06°C or 0.31°C. The larger discrepancy between the methods for temperature is likely due to the significant role of downward sensible heat flux near the top of the boundary layer. Though the WM method is probably the more accurate, the L1 method is the one that most represents the effects from surface fluxes and will therefore be the one used in the subsequent discussions.

The increases are small values, and would only produce a 0.1-0.3 K and 0.5-0.8 K increase in θ and θ_e, respectively. A shallower boundary layer would produce proportionally greater increases, but the data does not argue for this. However, the fluxes could increase somewhat as the air approaches the shore, since the SST increases slightly shoreward. **Therefore, we estimate that an increase of 1 K in θ_e occurs along the trajectory to the coast.**

The changes estimated from the fluxes are in excellent agreement with the offshore and nearshore observations. The cross-section in the Santa Barbara Channel shows that the maximum warm sector θ_e just ahead of the secondary cold front is 317 K (Fig. 3b), a one degree increase from that measured with the same airborne instruments 2-2.5 hours earlier and shown in Fig. 3a. In addition, the peak θ_e value of 318 K just to the west of the blocking front in Fig. 3b is 1 K greater than that in the corresponding location in Fig. 3a. This remarkable agreement may be fortuitous, although the fact that the airborne verification data was obtained at the right time at the right location for the estimated landfall of the sampled upwind air parcel lends strong credence to this result.

Another perspective shows that the additional moisture added during this final 140-km transit to the coast over the warmer coastal water is only 1-2% of the total water content of the air arriving at the coast. **Hence, the direct contribution to the coastal precipitable water appears to be small.**

Table 2: *Warm sector changes in specific humidity (q) and temperature (T) based on observed fluxes for each layer and for the entire 600 m deep boundary layer. For the entire boundary layer, results from the weighted-mean (WM) and the first layer (L1) methods are shown.*

Height layer	Mean height	Δq	ΔT
(m)	(m)	(g/kg/2.5 hr)	(K/2.5 hr)
0-66	33	0.00	0.00
66-285	175.5	-0.14	0.62
285-427	356	-1.51	2.15
427-590	508.5	2.04	-1.60
590-1154	872	-0.16	-0.24
0-600 (WM)	300	0.15	0.31
0-600(L1)	300	0.16	0.06

Effects of surface fluxes on convective available potential energy (CAPE)

Warming and moistening of the lowest few hundred meters makes a larger impact on destabilizing the air being forced to ascend the steep coastal mountains and the secondary cold front at the coast. We compute the offshore CAPE from the dropsondes and low-level aircraft measurements, and the nearshore CAPE by assuming that the only changes in the sounding occur in the BL and are due to the surface fluxes (Fig. 5). The results show that the 1 K increase of boundary-layer θ_e increases the CAPE by 27% from 321 Joules to 408 Joules. Hence, the coastal surface fluxes substantially decrease the stability and thereby contribute significantly to the very heavy, but brief, precipitation observed at Goleta (Fig. 6) and elsewhere along this part of the California coast (Fig. 7). This period of heavy precipitation resulted in flooding (Fig. 8).

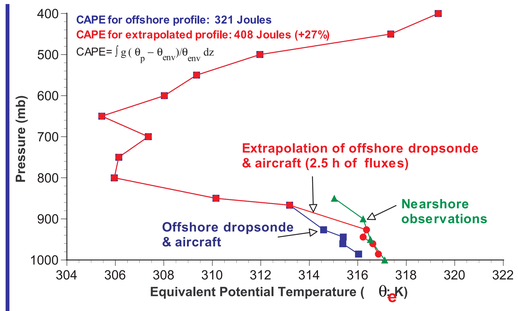

Fig. 5: Profiles of equivalent potential temperature (θ_e) for the offshore location (blue squares), extrapolation to the nearshore location using boundary layer changes due only to surface fluxes (red squares), and nearshore observations (green triangles). The equation for CAPE and the CAPE calculation results for the offshore and extrapolated nearshore profiles are shown at upper left. θ_p and θ_{env} are the parcel and environmental potential temperatures, respectively.

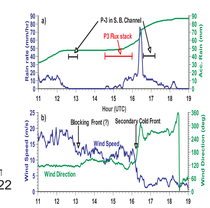

Fig. 6: Surface observations at Goleta. Shown are a) rain rate and accumulated rainfall, and b) wind speed and direction.

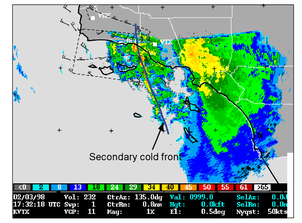

Fig. 7: NEXRAD image from Ventura (VTX) at 1732 UTC Feb. 3. showing the intense convection where the secondary cold front intersects the northern coastline of the California Bight. The front-relative P-3 track is dashed.

Fig. 8: Flooded streets near Goleta airport at about 1800 UTC Feb. 3, 2002. Photo by P. Neiman.

4. EXTENSION TO NON-EL NIÑO YEARS

Method:

a) Use surface flux parameterizations of Fairall *et al*. (1996)

b) Compute the surface H_s, H_l, and expected 2.5-hour change in θ_e for a range of sea-surface temperatures which included both the observed El Niño values and the values typical for non-El Niño years (Fig. 9).
- assume that BL conditions same as that observed for the Feb. 3 case.

Results:

a) for the observed El Niño conditions, parameterization does a good job at predicting the observed surface fluxes and the change in BL θ_e (Fig. 9). Hence, the model appears reliable.

b) for SSTs representative of non El Niño years, H_s was substantially negative and H_l was positive but smaller. Hence, the change in θ_e is predicted to be near zero or slightly negative. **That is, the coastal surface fluxes are not expected to contribute to the destabilization of the boundary layer during landfalling storms in a non-El Niño year, even though they do contribute during El Niño years.** They might even lead to slight stabilization.

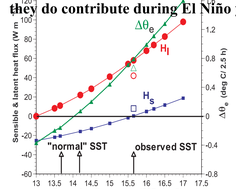

Fig. 9: Sensible heat flux (blue line), latent heat flux (red line), and associated change in the boundary layer θ_e (green line) as a function of sea-surface temperature (SST). The computations of H_s, H_l and $\Delta\theta_e$ were done using the bulk algorithm of Fairall et al *(1996) and assuming conditions as observed in the offshore warm sector on Feb. 3 (z=66 m, ws=13.4 m/s, T=14.9°C, RH=87%, p=985.7 mb, zi=600 m). Also shown are the observed covariance H_s (open blue box), H_l (open red circle) and $\Delta\theta_e$ (open green triangle). The observed SST and those from more normal years are marked by arrows along the bottom.*

5. CONCLUSIONS

This paper shows that:

a) the observed surface sensible and latent heat fluxes within 150 km of the shore within a moderate low-level jet **do not** contribute significantly to the precipitable water amount but **can** significantly contribute to the destabilization of the air just before it is forced to ascend at the cold front and the steep coastal terrain. As the air ascends in this case, deep convection occurs with significant coastal flooding as result.

b) the coastal fluxes only enhance the coastal precipitation during years with anomalously warm coastal sea-surface temperatures (ENSO years) and may even help suppress coastal convection during years of more normal colder SSTs.

Hence, during El Niño years when coastal waters are anomalously warm by 1.5-2.5°C, surface heat fluxes near the California coast can contribute to the coastal precipitation. During non-El Niño years, they are much less likely to do so unless the air temperatures in the storms are significantly colder.